Euler Analysis of Transonic Propeller Flows

J. M. Barton* and O. Yamamoto†
Sverdrup Technology Inc., Middleburg Heights, Ohio
and
L. J. Bober‡
NASA Lewis Research Center, Cleveland, Ohio

A three-dimensional Euler code, previously developed for high-speed propellers, was rewritten and vectorized for the Cray computer. First-order accurate, implicit integration was combined with approximate factorization, central differences, and constant coefficient dissipation to solve the unsteady, compressible Euler equations in general curvilinear coordinates. Calculations were compared with previous results and measurements. The new code required less memory and was more than two times faster than its predecessor. New boundary conditions produced more accurate results in terms of integrated performance characteristics. The code is a useful tool for examining the fluid dynamics and performance of propellers.

Nomenclature

A,B,C,D	= Jacobian matrices [Eq. (5)]
C_P, C_T	= power and thrust coefficient
e	= total energy per unit volume [Eq. (2)]
E,F,G,H	= Euler equations flux vectors [Eq. (1)]
I	= identity matrix [Eq. (5)]
J	= geometric Jacobian of the curvilinear transformation; also advance ratio
j,k,l	= indices along the (ξ,η,ζ) directions
N^{-1},P^{-1},S^{-1}	= transformation matrices arising from the diagonalization [Eq. (7)]
p	= static pressure
r	= cylindrical radial coordinate
R	= propeller radius
t	= nondimensional time variable
U	= Euler equations dependent variable vector
u,v,w	= cylindrical axial, radial, and circumferential velocity components
$\bar{u},\bar{v},\bar{w}$	= contravariant velocity components
z	= cylindrical axial coordinate
$\beta_{3/4}$	= blade angle at $r/R=0.75$
δ,Δ	= finite-difference central and forward-difference operators, respectively
ζ	= transformed curvilinear coordinate in the blade-to-blade direction (Fig. 2)
η	= transformed curvilinear coordinate in the hub-to-tip direction (Fig. 2)
$\Lambda_A,\Lambda_B,\Lambda_C$	= diagonal matrices of the corresponding Jacobian matrices A, B, C [Eq. (7)]
μ	= finite-difference averaging operator
ξ	= transformed curvilinear coordinate in the axial direction (Fig. 2)
ρ	= density
τ	= transformed time variable
ϕ	= cylindrical circumferential coordinate
ω	= propeller angular velocity

Superscripts

$n,n+1$	= integration time levels for current and advanced times, respectively
$()^*,^{**},^{***}$	= tentative values of quantities used during integration

Subscripts

t,τ	= partial derivatives with respect to time
j,k,l	= values of quantities at specific mesh location (j,k,l)
z,r,ϕ	= partial derivatives with respect to the cylindrical independent variables
ξ,η,ζ	= partial derivatives with respect to the curvilinear independent variables

Introduction

MANY studies published since 1975 have elaborated and documented the economic benefits of a modern technology propeller, relative to a comparable technology turbofan engine, as the propulsion system for subsonic aircraft with cruise Mach numbers up to 0.8.[1,2] The propeller operates transonically with a relative tip Mach number near 1.15. There are commonly 8-10 blades, each thin, swept, tapered, and twisted. The spinner and nacelle are area ruled to reduce compressibility losses. Propellers currently in use have straight blades, which are fewer in number and thicker, and experience diminished efficiency at Mach numbers above 0.6-0.65. The dramatic change in propeller geometry and operating conditions has necessitated establishment of a data base to support propeller design work. The data base is required to aid in understanding the effects of number of blades, sweep, twist, thickness, Mach number, and spinner contouring on the aerodynamic, acoustic, and aeroelastic performance.

The required information has been obtained primarily from model tests. Many phenomena, particularly acoustic and aeroelastic, do not scale reliably and require larger-scale testing, such as the effort underway between NASA, United Technologies, and Lockheed.[2] The large number of variables involved in the designs, the associated parametric model testing, the scaling uncertainties, and the large-scale testing are complex aspects of the design work and require accurate and flexible analysis methods for high-speed propellers, as discussed by Bober and Mitchell[3] and Bober and Chang.[4] Design, fabrication, and testing, at any scale, is time con-

Presented as Paper 85-1263 at the AIAA/SAE/ASME/ASEE 21st Joint Propulsion Conference, Monterey, CA, July 8-10, 1985; received Nov. 1, 1985; revision received Sept. 2, 1986.

*Director, Aeromechanics Department. Member AIAA.
†CFD Specialist, Aeromechanics Department. Member AIAA.
‡Deputy Chief, Propeller Aerodynamics and Acoustics Technology Branch. Member AIAA.

suming, subject to uncertainties, and expensive. Computational models can help mitigate these problems, as has been demonstrated in propulsion systems by Paynter[5] and in engine testing by Barton.[6] Measurements are required to establish the accuracy and range of applicability of the computations. The analyses can then be applied with confidence within the same class of flows and geometries. Parametrics can be performed quickly and cheaply, relative to testing, and the various phenomena can be examined in great detail. Caution must be exercised, however, when considering new classes of geometries and flows until measurements are obtained for validation purposes. The objective of this paper is to describe and evaluate modifications to an Euler equations solver with the goal of producing an accurate method for analyzing propeller flowfields.

Background

Methods for analyzing propeller flows date from the formulation and approximate solution of Prandtl and Betz[7] and the exact solution of Goldstein.[8] The propeller consisted of a finite number of straight, lightly loaded blades in a single row. A helical coordinate system was chosen and the wake was specified as a rigid helix having constant pitch. Each blade was represented by a single-bound vortex line, with the trailing vortices constituting the helical wake. The flow upstream of the propeller was uniform and incompressible. The problem then reduced to a two-dimensional solution of Laplace's equation for the velocity potential far downstream. The new high-speed propellers violate the assumptions of the early methods; thus, singularity methods were developed, usually for incompressible flow with a compressibility correction added. These methods produced solutions to the incompressible potential equation[9-11] or the linearized, compressible potential equation.[12,13] Solutions were also published for the transonic small-disturbance equation[14] and the transonic full potential equation[1,15] for propeller applications.

Solutions to the Euler equations for propeller flows have been reported by Celestina and Adamczyk,[16] Bober et al.,[17] Clark and Scott,[18] and Bousquet.[19] Celestina and Adamczyk applied the method of Jameson et al.[20] in cylindrical coordinates. Preliminary results at the design point for the SR-3 propeller[1] compared favorably with measurements. Recent results were obtained by Celestina et al.[21] for counterrotating propellers, applying the ideas of Adamczyk.[22] Bober et al. employed the method of Beam and Warming[23] for the SR-3 propeller. Results for the SR-3 were generally acceptable, but the swirl was overpredicted and the power coefficient was likewise too large. Clark and Scott adapted the turbomachinery code of Denton[24] by moving the shroud wall out a distance of one to two propeller radii from the tip. No studies have yet been published to determine how far away the wall should be or to impose a nonreflecting condition in place of the wall. Bousquet applied the method of Brochet[25] and examined the effects of number of blades, Mach number, rotational speed, and hub contouring on performance. No comparisons were made with measurements.

Two viscous analyses have been published recently utilizing marching solutions of the parabolized Navier-Stokes equations. Govindan et al.[26] performed preliminary calculations for flow in the neighborhood of a propeller blade tip. The pressure field was obtained from a potential flow calculation and the blade geometry was highly simplified. The entire hub region was neglected and only laminar solutions were published. The results did demonstrate the ability to produce (qualitatively, at least) a tip vortex with a space marching method. The method was extended to compressible flow and applied to the SR-3 propeller.[27] No comparisons were made with measurements. Pouagare[28] applied the method of Schiff and Steger[29] for rotors. Calculations were in good agreement with analytical results of Morris[30] for laminar flow over helical propeller blades with no hub or nacelle.

Governing Equations

The governing field equations for three-dimensional unsteady, rotational, inviscid flow are written in cylindrical coordinates. (These equations are referred to hereafter as the Euler equations.) The cylindrical coordinate system is an absolute (nonrotating) reference frame. To facilitate calculations a general time-dependent mapping is applied and the equations are transformed to a rotating curvilinear coordinate system. The curvilinear system is defined such that the

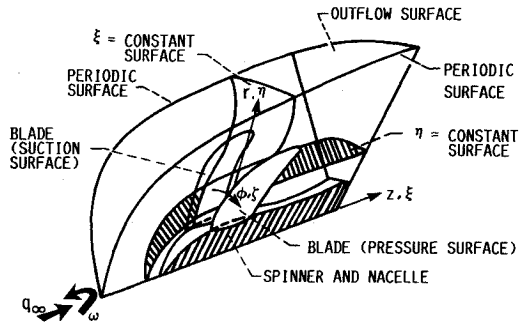

Fig. 1 Physical space.

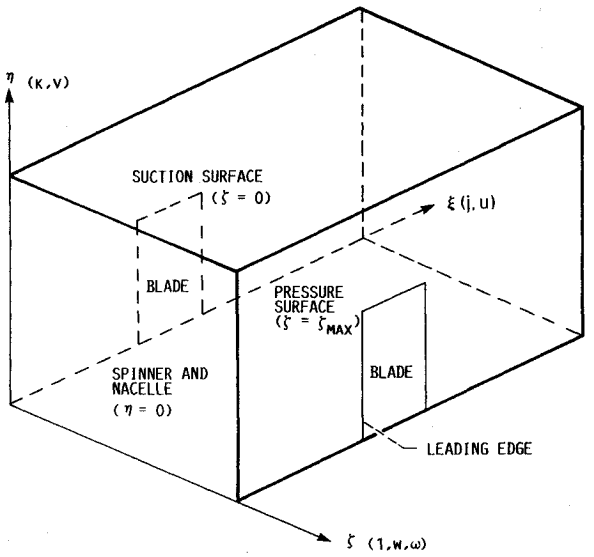

Fig. 2 Computational space.

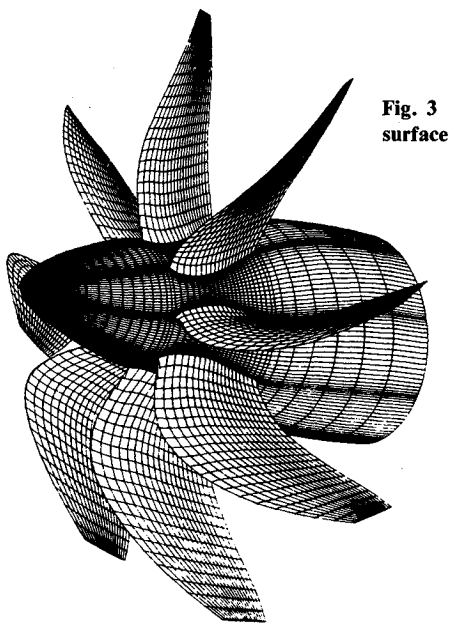

Fig. 3 SR-3 propeller with surface grid.

blades, spinner, and nacelle surfaces lie in constant coordinate planes. If (z,r,ϕ) are associated with the (cylindrical) axial, radial, and circumferential directions, respectively, the corresponding transformed coordinates are denoted by (ξ,η,ζ). The blades lie in ζ-constant planes and the spinner and nacelle lie in an η-constant plane. The flowfield is assumed to exhibit periodic symmetry in the blade-to-blade direction; thus, only the flow between two adjacent blades is considered. (Figures 1 and 2 illustrate the coordinate system and its relation to the computational space.)

For the assumptions stated (inviscid, rotational flow of a calorically perfect, nonheat conducting gas), the governing equations can be written in conservation law form as

$$\frac{\partial U}{\partial \tau}+\frac{\partial E}{\partial \xi}+\frac{\partial F}{\partial \eta}+\frac{\partial G}{\partial \zeta}+H=0 \tag{1}$$

where U is the vector of conserved quantities, E,F,G flux vectors, and H is a source term. The vectors are

$$U=\frac{1}{J}\begin{Bmatrix}\rho\\ \rho u\\ \rho v\\ \rho w\\ e\end{Bmatrix},\ E=\frac{1}{J}\begin{Bmatrix}\rho\bar{u}\\ \rho u\bar{u}+p\xi_z\\ \rho v\bar{u}+p\xi_r\\ \rho w\bar{u}+p\xi_\phi/r\\ (e+P)\bar{u}-p\xi_t\end{Bmatrix},\ F=\frac{1}{J}\begin{Bmatrix}\rho\bar{v}\\ \rho u\bar{v}+p\eta_z\\ \rho v\bar{v}+p\eta_r\\ \rho w\bar{v}+p\eta_\phi/r\\ (e+p)\bar{v}-p\eta_t\end{Bmatrix},\ G=\frac{1}{J}\begin{Bmatrix}\rho\bar{w}\\ \rho u\bar{w}+p\zeta_z\\ \rho v\bar{w}+p\zeta_r\\ \rho w\bar{w}+p\zeta_\phi/r\\ (e+p)\bar{w}-p\zeta_t\end{Bmatrix},\ H=\frac{1}{J}\begin{Bmatrix}\rho v/r\\ \rho uv/r\\ \rho(v^2-w^2)/r\\ 2\rho vw/r\\ (e+p)v/r\end{Bmatrix} \tag{2}$$

where J is the Jacobian of the coordinate transformation

$$J=\frac{\partial(\xi,\eta,\zeta)}{\partial(z,r,\phi)}\neq 0,\infty$$

The transformed system of equations is similar in appearance to the original system when written in terms of the contravariant velocity components, which are defined as

$$\begin{aligned}\bar{u}&=\xi_t+u\xi_z+v\xi_r+w\xi_\phi/r\\ \bar{v}&=\eta_t+u\eta_z+v\eta_r+w\eta_\phi/r\\ \bar{w}&=\zeta_t+u\zeta_z+v\zeta_r+w\zeta_\phi/r\end{aligned} \tag{3}$$

Geometric information is contained in the Jacobian J and in the metric terms. The metrics can be developed by applying the chain rule of differentiation and manipulating the resulting equations to obtain

$$\begin{aligned}\xi_z&=J(r_\eta\phi_\zeta-r_\zeta\phi_\eta),\ \xi_r=J(z_\zeta\phi_\eta-z_\eta\phi_\zeta)\\ \eta_z&=J(r_\zeta\phi_\xi-r_\xi\phi_\zeta),\ \eta_r=J(z_\xi\phi_\zeta-z_\zeta\phi_\xi)\\ \zeta_z&=J(r_\xi\phi_\eta-r_\eta\phi_\xi),\ \zeta_r=J(z_\eta\phi_\xi-z_\xi\phi_\eta)\\ \xi_\phi&=J(z_\eta r_\zeta-z_\zeta r_\eta),\ \xi_t=-(z_\tau\xi_z+r_\tau\xi_r+\phi_\tau\xi_\phi)\\ \eta_\phi&=J(z_\zeta r_\xi-z_\xi r_\zeta),\ \eta_t=-(z_\tau\eta_z+r_\tau\eta_r+\phi_\tau\eta_\phi)\\ \zeta_\phi&=J(z_\xi r_\eta-z_\eta r_\zeta),\ \zeta_t=-(z_\tau\zeta_z+r_\tau\zeta_r+\phi_\tau\zeta_\phi)\end{aligned} \tag{4}$$

In the current application, motion of the coordinates takes place in only one direction, the ζ direction; thus $z_\tau=r_\tau=0$ and $\phi_\tau=\omega$, the rotational velocity of the propeller. The metric ζ_t then becomes $-\omega\zeta_\phi$.

All variables are dimensionless, with velocities normalized by $a_\infty/\sqrt{\gamma}$, angular velocity by $D\sqrt{\gamma}/a_\infty$, pressure by p_∞, density by ρ_∞, lengths by D, and total energy by $\rho_\infty a_\infty^2/\gamma$.

Numerical Method

Following the development in Refs. 17 and 31, the transformed equations are treated as a system of coupled, first-order, autonomous differential equations. First-order accurate implicit Euler time differencing is employed and the flux vectors are linearized by Taylor series expansions up to second order in time. The equations can be written as

$$\left[I+\Delta\tau\left(\frac{\partial A}{\partial \xi}+\frac{\partial B}{\partial \eta}+\frac{\partial C}{\partial \zeta}+D\right)\right]^n\Delta U=-\Delta\tau\left[\frac{\partial E}{\partial \xi}+\frac{\partial F}{\partial \eta}+\frac{\partial G}{\partial \zeta}+H\right]^n \tag{5}$$

where I is the identity matrix, $\Delta U=U^{n+1}-U^n$, and

$$A^n=\frac{\partial E^n}{\partial U^n},\ B^n=\frac{\partial F^n}{\partial U^n},\ C^n=\frac{\partial G^n}{\partial U^n},\ D^n=\frac{\partial H^n}{\partial U^n} \tag{6}$$

are the Jacobian matrices resulting from the linearization. (See Ref. 32 for details of the linearization.) The left-hand side of Eq. (5) is factored into three one-dimensional operators with the formal order of accuracy of the algorithm retained. The resulting operators involve block tridiagonal inversions. Since attainment of a steady-state solution is the ultimate goal of the effort, the left-hand side of Eq. (5) is regarded as an iteration operator and is manipulated to reduce the total operation count and to accelerate convergence. One step toward this end is neglecting the nonhomogeneous D. The second step is to diagonalize the Jacobian matrices of Eq. (6) using a similarity transformation.[17,31-34] (The development is contained in Ref. 32.) Subsequently, the spatial derivatives are replaced by central differences and appropriate one-sided differences at the boundaries. The equations are now written as

$$\begin{aligned}[I+\Delta\tau\delta_j\Lambda_A]\Delta U^{***}&=S_\xi{}^{-1}-\Delta\tau[\mu_j\delta_jE+\mu_k\delta_kF+\mu_l\delta_lG+H]\\ [I+\Delta\tau\delta_k\Lambda_B]\Delta U^{**}&=N^{-1}\Delta U^{***}\\ [I+\Delta\tau\delta_l\Lambda_C]\Delta U^{*}&=P^{-1}\Delta U^{**}\\ \Delta U&=S_\xi\Delta U^{*}\\ U^{n+1}&=U^n+\Delta U\end{aligned} \tag{7}$$

The subscripts j, k, and l represent the ξ, η, and ζ directions, respectively. The finite difference operator notation is defined as

$$\begin{aligned}\mu_jf&=0.5(f_{j+\frac{1}{2}}+f_{j-\frac{1}{2}})\\ \delta_jf&=f_{j+\frac{1}{2}}-f_{j-\frac{1}{2}}\\ \Delta f^n&=f^{n+1}-f^n\end{aligned}$$

The mesh increments in the transformed plane are uniform and specified as unity, i.e., $\Delta\xi=\Delta\eta=\Delta\zeta=1$. The quantities

Λ_A, Λ_B, and Λ_C are diagonal matrices whose components are the eigenvalues of the Jacobian matrices A, B, and C. The S, N, and P matrices also result from the diagonalization and are contained in Ref. 32. The benefit of the effort is that the five equations are uncoupled and can be solved by five passes through a scalar tridiagonal matrix solver (for each direction). The original block inversions have been eliminated with an approximate reduction of 30% in solution time. The sacrifice is that the transient is no longer physically meaningful, regardless of the magnitude of the stepsize.

The boundary conditions are representative of the propeller in an infinite ambient fluid. The flow is assumed to be cyclic around the propeller, so that the computational domain contains only one blade passage. Figure 2 illustrates the transformed space and its correspondence to physical space. Figure 1 indicates the specific computational boundaries. The domain is actually "warped spherical," as used by Bober et al.[17] and Pulliam and Steger,[35] and not cylindrical. On the periodic surfaces beyond the blade tip, upstream of the leading edge, and downstream of the trailing edge, the governing equations are solved implicitly as they are in the interior. A periodic tridiagonal matrix inversion is employed in the circumferential direction. The spinner, nacelle, and blades are impermeable. The impermeable (tangency) condition on solid surfaces is enforced by extrapolating the contravariant velocities to the surface, setting the appropriate contravariant velocity component to zero ($\bar{v}$ for spinner/nacelle and $\bar{w}$ for blades), and computing the corresponding physical velocities from the inverse of Eq. (3). Pressure and density are also extrapolated to the surface. At the inflow and other boundaries ($\eta = \eta_{max}$), the dependent variables are specified from freestream conditions. The axis of symmetry ($\xi = 0$) requires that $v = w = 0$ and that radial derivatives of all other quantities are zero.

At outflow, $\xi = \xi_{max}$, the transformed radial momentum equation is simplified by neglecting the radial velocity and dropping the unsteady term. The remaining equation is solved for the radial pressure distribution by a trapezoidal rule integration, starting from a specified value at the freestream boundary. Since the integration is effected along every radial line in the outflow plane, the dependent variables can vary circumferentially as well as radially. The outflow plane is located two radii from the trailing edge. (The solutions were nearly identical when the outflow was placed four radii downstream.) The three velocity components and density are extrapolated from upstream (zero first derivative). This outflow treatment is sometimes referred to as radial equilibrium.

For a steady-state solution, the specification of the initial conditions is theoretically arbitrary, at least for linear systems of equations. In the current work, freestream conditions are imposed everywhere.

Applications

The Euler analysis is applied to the flowfield of the SR-3 propeller[36] at several operating conditions. (The nominal Reynolds number of the model-scale tests was 1.5×10^7/m and the propeller diameter was 0.62 m.) Results are compared with measurements and previous calculations where available. In all cases, the blade geometry used included the centrifugal loading effects experienced during operation. The centrifugal effects were determined using a finite-element structural analysis code for the propeller operating at a Mach number of 0.8 and advance ratio of 3.06. At other rotational speeds and Mach numbers, the deflection was scaled between the static and the design point geometry.

Performance parameters are obtained by integrating the blade pressure distribution to obtain the net force. The resultant force is then resolved into thrust and torque components, from which the power coefficient is computed. Efficiency is calculated as the product of advance ratio and thrust coefficient divided by power coefficient.

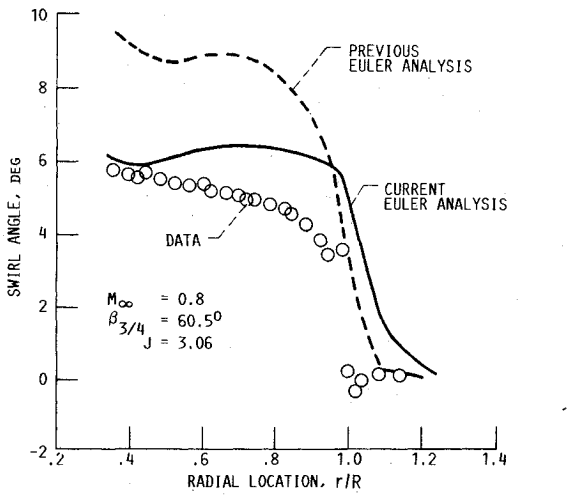

Fig. 4 Swirl angle comparisons for the SR-3 propeller 0.03 radii downstream of the trailing edge.

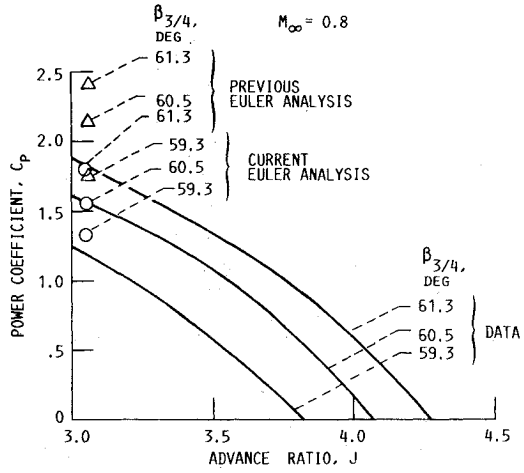

Fig. 5 Power coefficient comparisons for the SR-3 propeller.

The SR-3 propeller is pictured in Fig. 3 with a surface grid present. The grid is concentrated about the leading and trailing edges and the tip. The inflow boundary is located about 10 propeller radii upstream of the leading edge, the outflow boundary is 2 radii downstream of the trailing edge, and the freestream boundary is 9 radii from the tip. The mesh was generated as a sequence of two-dimensional planes using an elliptic mesh generator.[31] The mesh in an r-z plane was generated, encompassing one surface (suction or pressure) of the blade. The mesh was rotated about the propeller axis in specified increments. The mesh containing the opposing blade surface was then generated to complete the requirements. This approach for producing a grid resulted in two of the metrices of Eq. (4) being identically zero—ξ_ϕ and η_ϕ.

The code described in Ref. 31 underwent several modifications (vectorization for the Cray computer, implementation of new boundary conditions, and inclusion of a new solver) and results from the new code were compared with the original results. The initial calculations were performed for the same mesh used in the original work: 45 points axially, 21 points radially, and 11 points circumferentially ($45 \times 21 \times 11$), with 250 points on each blade surface. Subsequent calculations were made with the new version using a more refined mesh ($51 \times 41 \times 21$), but retaining the same computational boundaries. The refined mesh had 1000 points on each blade surface.

The code vectorization involved four steps: 1) restructuring the indexing, 2) restructuring some DO-LOOPS, 3) put-

ting small subroutines directly inline, and 4) recoding the tridiagonal solvers. The vectorization reduced execution times by a factor of two. (The resultant code also ran faster on a scalar machine.)

Two boundary condition changes were made. Formerly, the variables on the periodic boundary were obtained by linearly averaging values on both sides of the boundary. This was replaced by an implicit solution of the field equations for all periodic points, using a periodic scalar tridiagonal solver. Calculations produced monotonic convergence of the solution where previously the decay of the error was oscillatory. At the outflow boundary, a characteristic approach was used originally with a specified static pressure. The pressure was imposed as constant and uniform throughout the outflow plane, however, which artificially produced large swirl velocities. (The outflow boundary was located two radii downstream of the propeller.) The characteristic analysis was replaced by a radial equilibrium treatment, with the static pressure prescribed at the freestream boundary and computed elsewhere. All other variables were extrapolated from the interior. The result was a much reduced swirl velocity, as seen in Fig. 4. (The present calculations do exhibit worse agreement in the tip region.) An attendant reduction in predicted power coefficient was also realized. Figure 5 includes three data points for fixed advance ratio ($J=3.06$). In comparing efficiency for the same conditions, at $\beta_{3/4}=59.3$ deg, $\eta=80.3$ (79.3 measured); at $\beta_{3/4}=60.5$ deg, $\eta=76.6$ (79.5 measured); and at $\beta_{3/4}=61.3$ deg, $\eta=74.1$ (78.0 measured). The current results are in good agreement with the measurements. Figure 6 shows the crossflow velocity vectors 0.03 radii downstream of the trailing edge. The tip vortex diffuses less on the finer grid relative to results from Ref. 17. In addition, the computed power coefficient was 1.54 with the denser grid, compared to 2.2 formerly.[17] The measured value was 1.54.[36]

To further increase efficiency, alternatives to the original FORTRAN tridiagonal solver were examined. An assembly language scalar tridiagonal solver was implemented in place of the FORTRAN nonperiodic solver, producing a 10% reduction in CPU time. For comparison, the FORTRAN solvers, periodic and nonperiodic, were rewritten for vectorization. Vectorization can result from performing multiple tridiagonal inversions along parallel mesh lines. The increase in storage for the extra matrix coefficients is very small. The resulting vectorized FORTRAN code is 20% faster than the assembly language solver.

The remaining calculations were all run until the L_2 norm of the residual decayed two to three orders of magnitude. The typical run required 0.000076 s per mesh point per step. The calculations employed 2000 steps; however, the convergence history indicated satisfactory (at least two orders of magnitude) residual decay between 500 and 1000 steps.

Figure 7 presents the power coefficient as a function of advance ratio at a Mach number of 0.8. The present results are compared with measurements of Ref. 36. The Euler results are in close agreement with the measurements. Recalling that the results are inviscid, however, one must conclude that the power is still somewhat overpredicted. (The power required inviscidly should be less than the power required for viscous flows.) The overprediction is probably attributable to too much dissipation and inaccurate wall boundary conditions.

The new code, in general, produced more accurate results (when measured in terms of the integrated performance parameters), required somewhat less memory, and ran more than two times faster than the original. Within these limitations, the results demonstrate the design and off-design capability of the code for propeller analysis. The results are built upon the earlier work reported in Refs. 17 and 31. Further refinements and considerations are in progress. The nonlinear smoothing of Jameson as described by Pulliam[37] has been incorporated to enhance stability and improve

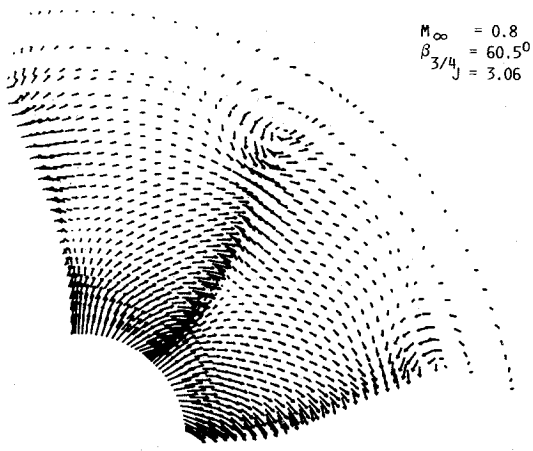

Fig. 6 Predicted cross-flow velocity vectors for the SR-3 propeller (51×41×21 grid).

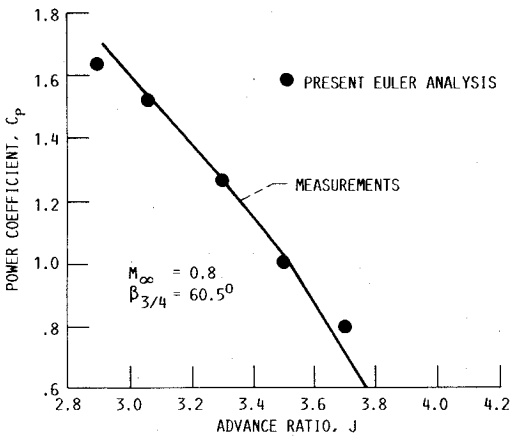

Fig. 7 Power coefficient comparisons for the SR-3 propeller.

calculations where shocks are present. Wall boundary conditions are now enforced through a method of characteristics approach. Both of these changes should improve accuracy and convergence and are reported in Ref. 38. Finally, a multistage Runge-Kutta version of the code is being developed and shows much potential.[39]

One of the remaining needs is improved three-dimensional grid generation capability. Obtaining a satisfactory grid is currently the most difficult step in modeling the flow and each operating condition requires a new grid. For example, for a fixed static blade angle, a change in either Mach number or rotational velocity produces a change in the deflected blade angle; thus, a new grid must be generated. (Propeller performance is quite sensitive to small changes in blade angle.) A means of quantifying the necessary qualities of a grid, and incorporating the criteria into a feedback loop in the generation process, is required. For instance, limits on grid skewness, variation of Jacobian from point to point, and variation in grid spacing from point to point are relevant variables. Removing some of the trial-and-error effort in producing a suitable grid would reduce the time to achieve a flowfield solution. This goal becomes even more pressing when extending the analysis to viscous solutions and counter-rotating propellers.

Acknowledgments

This research was supported by the NASA Lewis Research Center under Contract NAS3-24105. The authors would like to thank Dr. Endwell Daso of Sverdrup for performing the Euler calculations in Fig. 7, and Ms. Angela Quealy of Sverdrup for coding the vectorized tridiagonal solvers.

References

[1]*Aerodynamics and Acoustics of Propellers,* AGARD-CPP-366, Oct. 1984.

[2]Whitlow, J. B. Jr. and Sievers, G. K., "Fuel Savings Potential of the NASA Advanced Turboprop Program," NASA TM-83736, Sept. 1984.

[3]Bober, L. J. and Mitchell, G. A., "Summary of Advanced Methods for Predicting High Speed Propeller Performance," AIAA Paper 80-0225, Jan. 1980.

[4]Bober, L. J. and Chang, L. K., "Factors Influencing the Predicted Performance of Advanced Propeller Designs," AIAA Paper 81-1504, July 1981.

[5]Paynter, G. C., "CFD Technology for Propulsion Installation Design—Forecast for the 80's," *Journal of Engineering for Power,* Vol. 104, No. 4, Oct. 1982, pp. 832–837.

[6]Barton, J. M., "The Role of CFD in Aeropropulsion Ground Testing," *Journal of Aircraft,* Vol. 21, Oct. 1984, pp. 745–750.

[7]Prandtl, L. and Betz, A., "Vier Abhandlungen zur Hydrodynamik und Aerodynamik," Göttingen, FRG, 1927.

[8]Goldstein, S., "On the Vortex Theory of Screw Propellers," *Proceedings of the Royal Society of London,* Vol. A123, No. 792, Jan. 1929, pp. 440–465.

[9]Chang, L. K. and Sullivan, J. P., "Optimization of Propeller Blade Twist by an Analytical Method," *AIAA Journal,* Vol. 22, Feb. 1984, pp. 252–255.

[10]Egolf, T. A., Anderson, O. L., Edwards, D. E., and Landgrebe, A. J., "Propeller-Nacelle Aerodynamic Performance Prediction: Vol. 1, Theory and Initial Application and Vol. 2, User's Manual for the Computer Program," United Technologies Research Center, East Hartford, CT, R79-912949-19, 1979.

[11]McCormick, B. W., Aljabri, A. S., Jumper, S. J., and Martinovic, Z. N., "The Analysis of Propeller Aerodynamics and Noise," SAE Paper 790576, April 1979.

[12]Hanson, D. B., "Compressible Helicoidal Surface Theory for Propeller Aerodynamics and Noise," *AIAA Journal,* Vol. 21, June 1983, pp. 881–889.

[13]Schulten, J.B.H.M., "Aerodynamics of Wide-Chord Propellers in Non-Axisymmetric Flow," AGARD-CPP-366, Oct. 1984, pp. 7-1–7-10.

[14]Rae, W. J., "Computer Program for Relaxation Solutions of the Nonlinear Small-Disturbance Equation for Transonic Flow in an Axial Compressor Blade Row," AFOSR-TR78-0855, April 1978.

[15]Jou, W. H., "Finite Volume Calculation of Three-Dimensional Flow around a Propeller," *AIAA Journal,* Vol. 21, Oct. 1983, pp. 1360–1364.

[16]Celestina, M. L. and Adamczyk, J. J., "Three-Dimensional Euler Solver for Turbomachinery," Paper presented at NASA Marshall SSME Computational Fluid Dynamics Workshop, Huntsville, AL, Nov. 1984.

[17]Bober, L. J., Chaussee, D. S., and Kutler, P., "Prediction of High Speed Propeller Flow Fields Using a Three-Dimensional Euler Analysis," AIAA Paper 83-0188, Jan. 1983.

[18]Clark, B. J. and Scott, J. R., "Coupled Aerodynamic and Acoustical Prediction for Turboprops," Paper presented at 107th Meeting of Acoustical Society of America, Norfolk, VA, May 1984.

[19]Bousquet, J. M., "Aerodynamic Methods Used in France for Designing Advanced High-Speed Propellers," *Recherche Aerospatiale,* No. 1985-1, 1985, pp. 1–15.

[20]Jameson, A., Schmidt, W., and Turkel, E., "Numerical Solution of the Euler Equations by Finite Volume Methods Using Runge-Kutta Stepping Schemes," AIAA Paper 81-1259, June 1981.

[21]Celestina, M. L., Mulac, R. A., and Adamczyk, J. J., "A Numerical Simulation of the Inviscid Flow Through a Counter-Rotating Propeller," ASME Paper 86-GT-138, June 1986.

[22]Adamczyk, J. J., "Model Equations for Simulating Flows in Multistage Turbomachinery," NASA TM-86869, Nov. 1984.

[23]Beam, R. M. and Warming, R. F., "Implicit Numerical Methods for the Compressible Navier-Stokes and Euler Equations," VKI Lecture Series 1981–82, von Karman Institute, Rhode Saint Genese, Belgium, 1982.

[24]Denton, J. D., "An Improved Time-Marching Method for Turbomachinery Flow Calculations," ASME Paper 82-GT-239, 1982.

[25]Brochet, J., "Numerical Computation of Three-Dimensional Transonic Internal Flows," *Recherche Aerospatiale,* No. 1980-5, 1980, pp. 3–18.

[26]Govindan, T. R., Levy, R. and Shamroth, S. J., "Computation of the Tip Vortex Generation Process for Ship Propeller Blades," Office of Naval Research, Final Rept. R83-920021-F, April 1984.

[27]Govindan, T. R. and Levy, R., "Computation of the Tip Vortex Flow Field for Advanced Propellers," SBIR Phase I-Final Report, to be published.

[28]Pouagare, M. C., "Numerical and Experimental Investigation of Turbomachinery Rotor Flow Fields," Ph.D. Thesis, Pennsylvania State University, University Park, Dec. 1984.

[29]Schiff, L. B. and Steger, J. L., "Numerical Simulation of Steady Supersonic Viscous Flow," *AIAA Journal,* Vol. 18, Dec. 1980, pp. 1421–1430.

[30]Morris, P. J., "The Three-Dimensional Boundary Layer on a Rotating Helical Blade," *Journal of Fluid Mechanics,* Vol. 112, 1981, pp. 283–296.

[31]Chaussee, D. S. and Kutler, P., "User's Manual for Three-Dimensional Analysis of Propeller Flow Fields," NASA CR-167959, Jan. 1983.

[32]Barton, J. M., Yamamoto, O., and Bober, L. J., "Inviscid Analysis of Advanced Turboprop Propeller Flow Fields," AIAA Paper 85-1263, July 1985.

[33]Chaussee, D. S. and Pulliam, T. H., "A Diagonal Form of an Implicit Approximate-Factorization Algorithm as Applied to the Calculation of the Inviscid and Viscous Supersonic Flow Fields of Two-Dimensional Inlets," AIAA Paper 80-67, Jan. 1980.

[34]Pulliam, T. H. and Chaussee, D. S., "A Diagonal Form of an Implicit Approximate Factorization Algorithm," *Journal of Computational Physics,* Vol. 39, 1981, pp. 347–363.

[35]Pulliam, T. H. and Steger, J. L., "Implicit Finite-Difference Simulations of Three-Dimensional Compressible Flow," *AIAA Journal,* Vol. 18, Feb. 1980, pp. 159–167.

[36]Rohrbach, C., Metzger, F. B., Black, D. M., and Ladden, R. M., "Evaluation of Wind Tunnel Performance Testing of an Advanced 45 Degree Swept Eight-Bladed Propeller at Mach Numbers From 0.45 to 0.85," NASA CR-3505, March 1982.

[37]Pulliam, T. H., "Artificial Dissipation Models for the Euler Equations," AIAA Paper 85-0438, Jan. 1985.

[38]Yamamoto, O., Barton, J. M., and Bober, L. J., "Improved Euler Analysis of Advanced Turboprop Propeller Flows," AIAA Paper 86-1521, July 1986.

[39]Barton, J. M. and Yoon, S., "Finite Difference Solution of the 3-D Euler Equations Using a Multistage Runge-Kutta Method," Paper presented at 10th International Conference on Numerical Methods in Fluid Dynamics, Beijing, China, June 1986.